Low-Voltage Field Ionization of Gases Up to Torr-Level Pressures Using Massive Arrays of Self-Aligned Gated Nanoscale Tips

Arash A. Fomani, *Member, IEEE*, Luis Fernando Velásquez-García, *Senior Member, IEEE*,
and Akintunde Ibitayo (Tayo) Akinwande, *Fellow, IEEE*

***Abstract*—Large arrays of self-aligned gated nanoscale tips (320 000 tips in 32 mm^2 with average radii <5 nm) are reported for application as gas ionizers in portable analytical instruments. The fabricated devices are capable of field ionization (FI) of gases at voltages < 150 V even for helium with the highest ionization potential among molecules. Reliable operation of the devices was demonstrated at pressures as high as 1 Torr in He and 10 Torr in N$_2$. FI at higher pressures was only prohibited by gas discharge rather than device failure. Ion currents as high as 0.35 nA in N$_2$ and 0.1 nA in He were generated at a tip-to-gate bias of 200 V. Continuous operation for 10^4 s at 10 Torr confirmed excellent stability of the device for FI of gases. The device characteristics slowly degraded during continuous operation possibly due to particle adsorption on the tip surface. The device characteristics can be restored by operating the device as a field emitter at pressures <10^{-7} Torr.**

***Index Terms*—Analytical instruments, field ionization (FI), gated tip arrays, self-aligned structure.**

I. INTRODUCTION

GAS FIELD ionizers are promising candidates as ion sources for portable analytical instruments due to low power-consumption, reliable operation at high (torr-level) pressures, and soft ionization capability. Unlike impact ionization techniques, field ionization (FI) provides an efficient method for producing stable molecular ions even from complex organic compounds. Consequently, field ion sources can generate nonfragmented ions for exact measurement of the mass to charge ratio of an analyte [1], [2]. These devices are used in various analytical instruments such as field ion mass spectrometers (FIMS) [3]–[6] and atom beam microscopes [7]. Other applications include gas chromatography FIMS for analysis of petroleum products [8] and neutron generators for detection of shielded nuclear material [9] and oil-well logging [10]. Despite the attractive features offered by field ion sources, long-term, reliable, and high pressure operation has not been reported due to high voltages (>500 V) needed for field ionization using the current state-of-the-art devices.

Conventional gas ionizers produce ions based on the electron impact ionization technique in which high-energy electrons collide with neutral molecules to create ions by fragmentation. These gas ionizers utilize either thermionic cathodes [11], [12] or field emission (FE) cathodes [13]–[15] as electron sources. In thermionic emission, electrons are excited above the vacuum level at filament temperatures above 2000 K. Consequently, thermionic sources require high power (>1 W) and must be operated at low pressures (<10^{-4} Torr) to prevent device degradation due to reaction with surrounding gas molecules [16]. Alternatively, in FE cathodes, electrons are extracted from the emitter by a field-assisted tunneling process [5]. The FE sources must be also operated at low pressures (<10 mTorr) to mitigate emitter degradation by back-streaming ions [17]. In contrast, field ion sources harness the FI phenomenon in which electrons tunnel out of a neutral gas molecule under the influence of an intense electric field produced by a sharp tip [5]. As the ionizer tip is biased at large positive voltages, it repels the positively charged ions. Consequently, the device can be operated at higher pressures. This is desirable for portable instruments, as the size and power consumption of the pump are reduced.

To initiate the FI process, the electric field surrounding the ionizer tip must lower the height and narrow the width of the potential barrier seen by an electron to allow tunneling. In addition, the electric field must raise the energy level of the electron to or above the Fermi level of the ionizer [see Fig. 1(a)]. These two conditions are expressed by [18]

$$F q x_c = I - \phi - q^2/4x_c \tag{1}$$

and

$$\tau_i(x_c) \cong \upsilon_e^{-1}\exp\left[6.8\times 10^7\left(I^{3/2}-\phi^{3/2}\right)\alpha_I/F\right] \tag{2}$$

where F is the electric field, I the first ionization potential of the gas molecule, ϕ the work function of ionizer, x_c the critical distance, τ_i lifetime of electron inside the gas molecule, α_I the image lowering factor, and υ_e the electron tunneling attempt frequency (~10^{15}–10^{16} Hz). For FI to occur, the dwell time

---

Manuscript received November 7, 2013; revised January 20, 2014; accepted February 28, 2014. Date of publication April 7, 2014; date of current version April 18, 2014. This work was supported in part by the Defense Advanced Research Projects Agency/Microsystem Technology Office under Contract W31P4Q-10-1-0005 and in part by the Microsystems Technology Laboratories, Massachusetts Institute of Technology. The review of this paper was arranged by Editor F. Ayazi.

A. A. Fomani and L. F. Velásquez-García are with the Microsystems Technology Laboratories, Massachusetts Institute of Technology, Cambridge, MA 02139 USA (e-mail: aafomani@mit.edu; lfvelasq@mit.edu).

A. I. Akinwande is with the Department of Electrical Engineering and Computer Science, Massachusetts Institute of Technology, Cambridge, MA 02139 USA (e-mail: akinwand@mtl.mit.edu).

Color versions of one or more of the figures in this paper are available online at http://ieeexplore.ieee.org.

Digital Object Identifier 10.1109/TED.2014.2310637

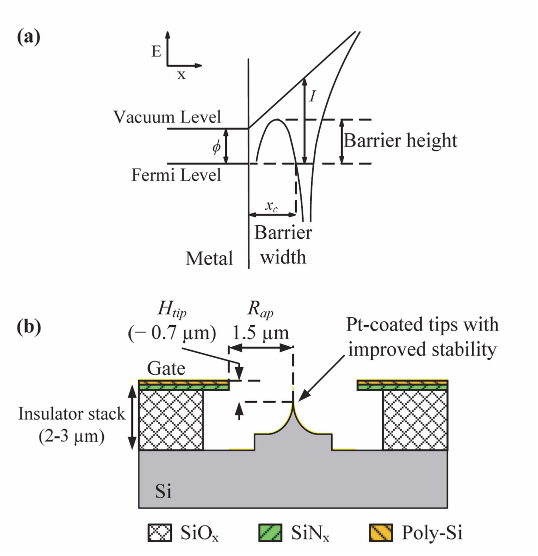

Fig. 1. (a) Potential-energy diagram of a gas molecule near the ionizer tip during the FI process and (b) cross-sectional schematic of the proposed self-aligned gated tip.

of a gas molecule at the vicinity of x_c must be comparable with τ_i. Assuming ionization takes place within 1 nm of x_c, the dwell time of the gas molecule can be estimated from thermal velocity of the molecule. Based on this simplified method, fields above 50 V/nm are estimated for ionization of He with $I = 24.6$ eV (tunneling probability $>10^{-3}$) while fields below 8 V/nm are approximated for a molecule with $I = 10$ eV. These field intensities agree with values derived by more rigorous methods (40 V/nm for He [18] and 7 V/nm for a typical organic molecule with $I = 10$ eV [4]) indicating that a field intensity in the range of 10^8 V/cm is required for FI.

In early FI experiments, gas ionization was performed at 5–20 kV biases using fine W wires (0.1 mm in diameter) sharpened by dipping into a molten salt or by electro chemical etching [19]. Later, 10-μm-thick W wires covered by carbon whiskers were used to enhance the ionization current by increasing surface area of the ionizer [4]. To further improve the ionizer performance, several methods such as electromigration caused by FE [20], growth of protrusion due to ion bombardment [21], and ion milling [22] were later used to sharpen the ionizer tip. Although these methods were not reproducible, they were able to lower the bias voltage for ionization to below 10 kV. In 1977, the first microfabricated device (volcano field ionizer) was presented by Aberth and Spindt that produced nA level currents with biases below 3 kV [23]. In more recent devices, a third electrode was integrated at close proximity of the ionizer tip to reduce the ionization voltage below 1 kV [15], [24]–[27]. These devices were made of carbon nanotubes [24], molybdenum [15], [25], tungsten on nickel posts [26], and tungsten coated Si tips [26], [27].

Despite these advances, state-of-the-art FI devices still require voltages >500 V to generate nA-range ion currents. High fields generated by such voltages severely undermine the lifetime and reliability of the device due to wear down of gate dielectric and electron emission from edge of the gate electrode [26]. Deposition of thick gate dielectric layers lowers the electric field inside the dielectric and mitigates the gate dielectric breakdown [27]. To suppress electron emission from the gate, a silicon nitride shield layer between the gate and tip [25] or a gate electrode with rounded edges [27] were employed. However, these approaches complicate the fabrication process and potentially reduce the yield. Furthermore, operation at torr-level pressures has not been reported. More importantly, to the best of our knowledge, the maximum dc field reported by gated tips is 24 V/nm with ionizer-gate voltages of 1000 V [26].

In this paper, we report low-voltage torr-level gas field ionizers with operating voltages as low as 150 V. The ionizer consists of large array of Pt-coated self-aligned gated Si tips (320 000 tips in 32 mm^2) with radii <5 nm and gate aperture radius of 1.5 μm. The tips were designed to generate fields above 20 V/nm at voltages lower than 200 V while the field at the edge of the gate remains below 0.2 V/nm. The device has a 2.5-μm-thick stack of silicon oxide/silicon nitride gate dielectric to limit the field intensity inside the gate dielectric to <100 V/μm allowing prolong operation of the device. Continuous FI is reported at pressures as high as 10 Torr with a slow decay over the course of a 10^4 s experiment.

II. STRUCTURE AND DESIGN OF THE FIELD IONIZER

The schematic of the field ionizer is shown in Fig. 1(b). The device has a Pt-coated silicon tip and an integrated gate electrode with 1.5-μm aperture radius. A stack of silicon oxide/silicon nitride with total thickness of 2–3 μm is employed as the insulator layer between the gate and silicon substrate. The device has a self-aligned configuration in which gate electrode is located symmetrically around the ionizer tip. When a positive voltage is applied between the ionizer tip and the gate, an electrostatic field is generated around the tip with the maximum intensity at the tip apex. At high enough voltages, electrons tunnel from the gas molecules to the tip. To collect the generated ions, a collector electrode biased at a negative voltage with respect to the gate terminal is positioned above the device. Because of the self-aligned configuration of the device, the field lines initiating from the tip terminate at the collector; consequently, the interception of generated ions by the gate electrode is avoided.

An ionizer that operates at voltages of <200 V needs a field factor (β) $> 10^6$ cm^{-1} for generating fields >20 V/nm, sufficient for ionizing even He, which has the highest ionization potential among molecules. In our devices, the important design parameters are the tip radius, R_{tip}, the height of the tip above the gate plane, H_{tip}, and the gate aperture radius, R_{ap}. R_{tip} is mainly determined by the fabrication method and processing conditions. For instance, in devices made of carbon nanofibers [24], the tip dimensions depend on the size of Ni seed used as the catalyst for carbon nanotube growth [28]; while in metallic tip devices [25]–[27], the tip radius is defined by metal deposition conditions. The fabricated tips in this paper have average radii <5 nm as

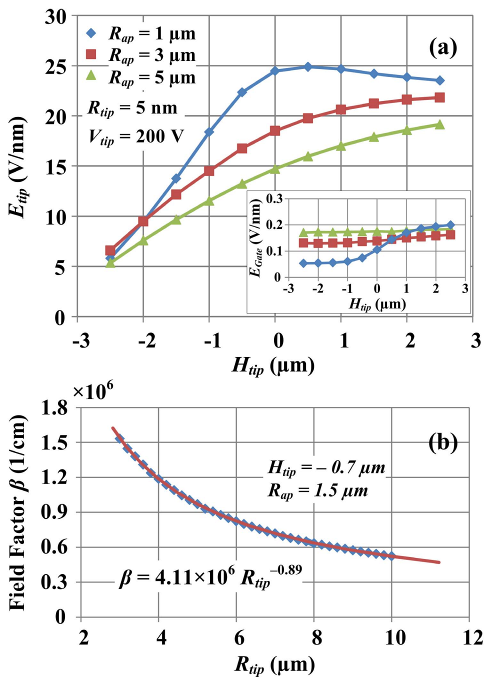

Fig. 2. (a) Simulated electrostatic field at the tip generated by a tip-to-gate bias of 200 V as a function of tip height, H_{tip}, with respect to the gate plane for different gate aperture radii, R_{ap}. Inset: the corresponding simulation results for the electrostatic field at the edge of the gate electrode. (b) Simulated field factor versus tip radius, R_{tip}, for a device with $R_{\text{ap}} = 1.5\ \mu$m and $H_{\text{tip}} = -0.7\ \mu$m (below the gate plane).

extracted from FE measurements and confirmed by SEM. Assuming $R_{\text{tip}} = 5$ nm, the electric field distribution was simulated by COMSOL in devices with different H_{tip} and R_{ap}. Fig. 2(a) shows the simulated electric field at the tip as a function of H_{tip} for devices with R_{ap} of 1, 3, and 5 μm at a tip-to-gate bias of 200 V. Shown in the inset of Fig. 2(a) is the corresponding simulated electric field at the edge of the gate. The negative values of H_{tip} correspond to devices with tips below the gate plane. As expected, the electric field is increased by reducing R_{ap} except when the tip is more than 2 μm below the gate plane ($H_{\text{tip}} < -2\ \mu$m). The electric field at the edge of the gate remains below 0.2 V/nm in all structures. For a $\beta > 10^6$ cm^{-1}, our simulations suggest a gated tip with $H_{\text{tip}} > -1\ \mu$m and R_{ap} of $\sim$1 μm. To simplify the device fabrication, the field ionizers consist of tips with H_{tip} of $-0.7\ \mu$m and integrated gate electrodes with R_{ap} of 1.5 μm. For this configuration, the simulated β is shown as a function of tip radius in Fig. 2(b). This curve can be used to estimate the tip radius using the field factor extracted from experimental results. A field factor in the range of 0.97–1.18 $\times$ 10^6 cm^{-1} is expected for devices with tip radii of 4–5 nm.

III. FABRICATION

Self-aligned gated tip arrays are fabricated using a three-mask process shown in Fig. 3 with details discussed in [29]. A brief summary of the fabrication process is as follows. First, a matrix of tall Si pillars embedded in SiO_x is created over the substrate by Si dry-etching, oxide deposition, and chemical mechanical polishing. This allows the incorporation of a thick gate dielectric with thicknesses $>2.5\ \mu$m in the device structure. Next, the exposed surfaces of the Si pillars are oxidized and covered by gate-stack layer comprised of SiN_x (300 nm), n-poly-Si (200 nm), and SiO_x (100 nm). Subsequently, the gate-stack is patterned to expose the oxide layer grown over Si pillars. The gate electrode and the oxide disk (etch stop) used for tip formation are then simultaneously defined in a single lithography/etching step to ensure a self-aligned gate and tip configuration. The nanometer-size tips are later formed by Si isotropic etching and oxidation sharpening [30]. The oxide layer over the tips is removed in buffered HF and a thin layer (10 nm) of Pt is e-beam deposited to improve the gate conduction as well as to protect the tips. It must be noted that, the n-poly-Si layer does not extend to the edge of SiN_x layer since dry etch of SiN_x is not selective to n-poly-Si and the n-poly-Si is oxidized during the oxidation sharpening step. However, the gate electrode is extended to the edge of the gate dielectric after Pt deposition. This further reduces the gate emission as Pt has a significantly higher work function ($\sim$6 eV) compared with n-poly-Si ($\sim$4.2 eV).

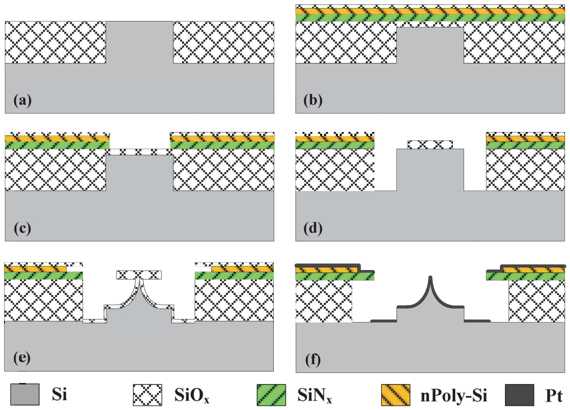

Fig. 3. Fabrication process flow of the proposed devices. (a) Si pillar etching, SiO_X deposition, and planarization, (b) oxide growth and gate-stack deposition, (c) via etching, (d) gate and oxide cap definition, (e) Si isotropic etching and oxidation sharpening, and (f) oxide etching and Pt deposition.

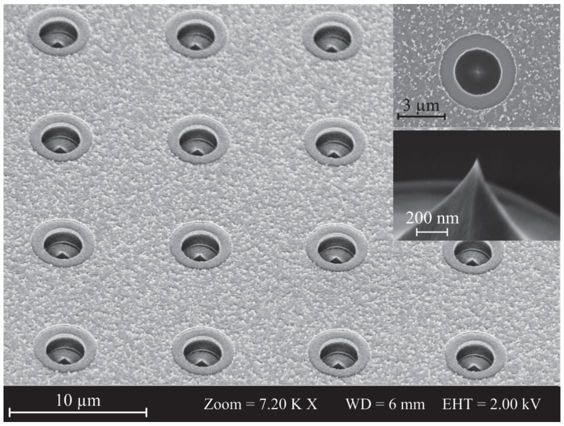

Fig. 4. SEM images of a self-aligned gated tip array.

SEM images of a fabricated field ionizer are shown in Fig. 4. The insets confirm the self-align structure of the device and nanometer-size tip dimensions. The array is 6 mm $\times$ 6 mm and consists of 320 000 gated tips with 10 μm center-to-center spacing. The gate contact is a 2 mm $\times$ 2-mm square located at the corner of the device while the emitter contact is made from the backside of the substrate.

IV. DEVICE CHARACTERISTICS

A. Field Factor

The field factor was extracted from FE characteristics of the device. In FE, electrons tunnel out of the surface of a material due to application of a high electric field that bends the vacuum level and decreases the width of the energy barrier. The Fowler-Nordheim (FN) equation calculates the emission current from supply rate of electrons to the surface and the tunneling probability across the potential barrier [31]. Assuming an effective emitting surface of α (cm^2), the emitted current (A) as a function of gate-to-emitter voltage, V_{GE} (V), effective field factor, β_{eff} (cm^{-1}), and the work function of tip material, ϕ (eV), can be approximated by [32]

$$I = a_{\mathrm{FN}} V_{\mathrm{GE}}^2 \exp\left(\frac{-b_{\mathrm{FN}}}{V_{\mathrm{GE}}}\right) \tag{3}$$

with

$$a_{\mathrm{FN}} = \frac{\alpha A \beta_{\mathrm{eff}}^2}{1.1\phi} \exp\left(\frac{10.4}{\phi^{1/2}}\right) \tag{4}$$

and

$$b_{\mathrm{FN}} = \frac{0.95 B \phi^{3/2}}{\beta_{\mathrm{eff}}} \tag{5}$$

where $A = 1.5 \times 10^6$ and $B = 6.87 \times 10^7$.

The terminal characteristics of the device operating as a field emitter are shown in Fig. 5(a). For this experiment, the gate was connected to ground and a negative voltage was applied to the tips. To collect the emitted electrons, a conductive plate was placed 1 cm above the device and biased at a positive voltage (100 V) with respect to the gate. The array produced more than 10 mA of emission current at gate-to-tip bias of 150 V while the intercepted current by the gate was less than 20 μA at maximum emission current. The device exhibited a high electron transmission through the gate ($>$99.5%) due to the self-aligned electrode configuration. The FN plot of the emitter current, $\log(I/V^2)$ versus V^{-1}, is shown in Fig. 5(b). The curve follows classical FN behavior at voltages $>$60 V, where the gate current is negligible compared with emitted current. The linearity of FN plot suggests that the supply of electrons is not limited at these current levels and the field penetration into the tips is negligible because of the metal coating of the tips. In contrast, the gate current does not exhibit FN behavior implying the current is due to gate dielectric leakage rather than interception of the emitted electrons. β_{eff} can be calculated from (5) and the slope of a line fitted to the linear region of the FN plot. The extracted value for β_{eff} is higher than 1×10^6 cm^{-1}. By comparing the extracted β_{eff} values with the simulated field factor for tips with different R_{ap} [see Fig. 2(b)], an average radius of 4–5 nm is estimated for the tips. This is in good agreement with the SEM studies specifying tip radii of less than 5 nm.

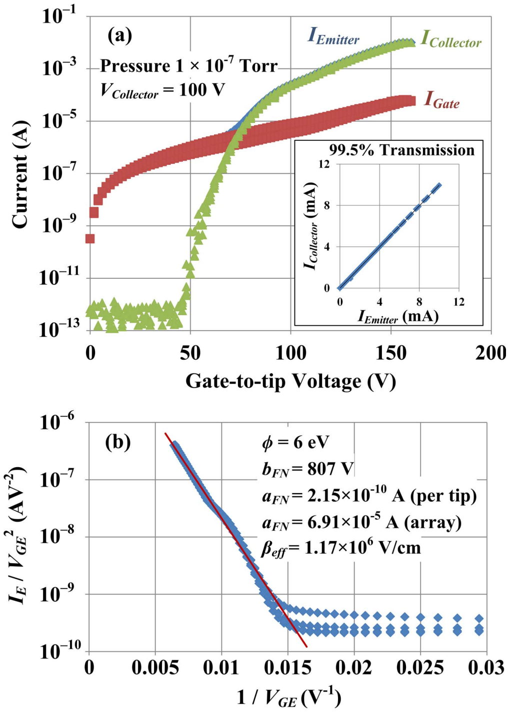

Fig. 5. (a) Terminal characteristics of a fabricated device as a function of gate-to-tip voltage during the FE mode of operation. The inset graphs the collected current versus the emitted current. (b) FN plot of the emitted current.

B. Field Ionization

FI measurements were performed using a positive voltage applied to the tips while the gate was connected to ground. A 2 cm × 2 cm piece of 10-$\Omega \cdot$cm Si placed 5 mm above the device was used as a collector for generated ions. Prior to pumping the chamber, the Si collector was RCA cleaned and HF-dipped to remove the native oxide. The chamber is then baked at 200 °C for 10 h while connected to the turbo pump. To further outgas the field ionizer and the collector, the device was operated as a field emitter with a constant current of 50 μA for 10 h.

FI of N_2 was performed at chamber pressures in the range of 0.1 mTorr to 10 Torr. The chamber pressure was set by controlling the flow rate of N_2 through a precision leak valve from MDC Vacuum Products (Hayward, CA). A negative voltage on the collector with respect to the gate is needed to collect the field ionized particles while a positive voltage is applied to the tips through the substrate. As the collector extends over the substrate beyond the gate region, the collector-gate bias must be $<$300 V to prevent plasma strike between the substrate and the collector at maximum tip (substrate) bias of 200 V. This is particularly important at 1–10 Torr pressures since the product of the chamber pressure and the collector-substrate distance is between 0.5 and 5 Torr $\cdot$ cm where the minimum of the Paschen curve for N_2 is located ($\sim$500 V at $\sim$2 Torr $\cdot$ cm) [33]. The Paschen curve presents the breakdown voltage of a gas between two parallel electrodes as a function of the electrodes' pressure-distance product (pd). A collector bias of -100 V with respect to the gate was employed for FI of N_2 at all pressures. This bias value was selected to be consistent with the experiments performed for FI of He.

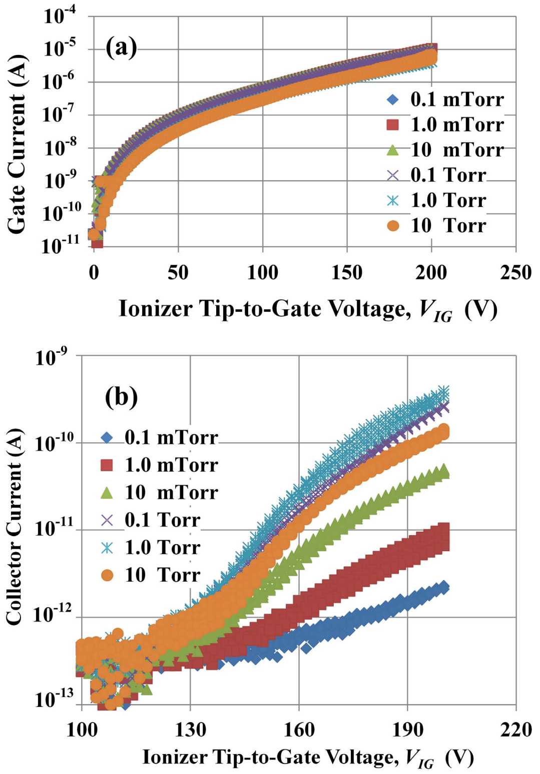

Fig. 6. FI of N_2. (a) Gate and (b) collector currents versus ionizer tip-to-gate bias.

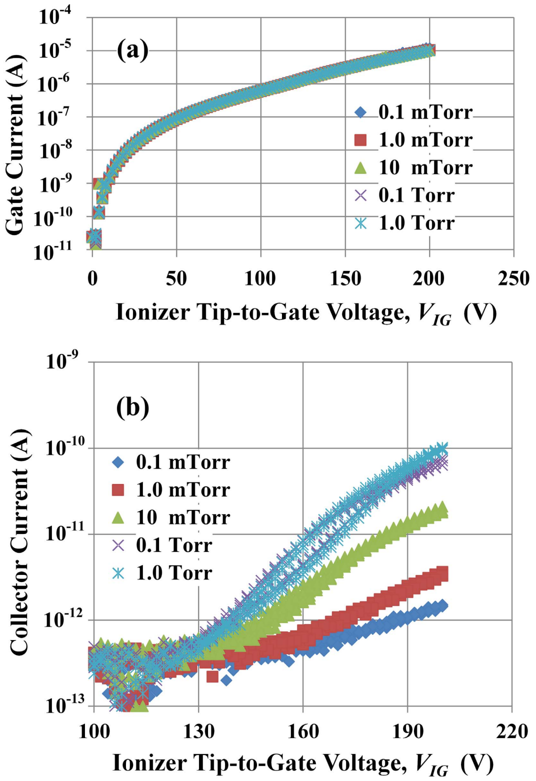

Fig. 7. FI of He. (a) Gate and (b) collector currents versus ionizer tip-to-gate bias.

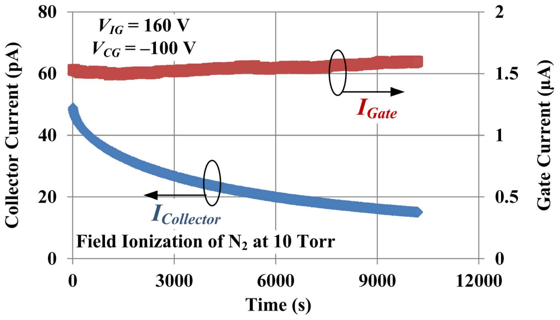

Fig. 8. Gate and collector currents over time during continuous field ionization of N_2 at 10 Torr.

The gate and collector currents as a function of potential difference between the ionizer tip and the gate, V_{IG}, are depicted in Fig. 6 for FI of N_2 at different pressures. The ion current monotonically increased with V_{IG}. With respect to the pressure, the ion current reached a maximum at pressures of ~1 Torr and then slowly decreased at higher pressures. Ion currents as high as 0.35 nA were generated at 1 Torr pressure and $V_{\mathrm{IG}} = 200$ V. The gate current was less than 10.5 μA under all bias and pressure conditions.

Fig. 7 shows the terminal characteristics of the device during FI of He at pressures in the range 0.1 mTorr–1 Torr. The device can generate ion currents as high as 0.1 nA at V_{IG} of 200 V and pressure of 1 Torr. The maximum gate current was ~10 μA and it was independent of the chamber pressure. The pressure and voltage dependence of the collector current is similar to the measured value in FI of N_2 up to 1-Torr pressure. The FI experiment could not be performed at 10 Torr using the present setup due to plasma ignition at $V_{\mathrm{IG}} > 150$ V even with a collector bias of 0 V. This is explained by substantially lower electrical breakdown of He compared with N_2. The Paschen curve of He [33] has a minimum of ~150 V at *pd* value of ~1 Torr · cm while the *pd* product in the experimental setup is 5 Torr · cm at 10 Torr. However, saturation of collector current was observed for He when pressure approached to 1 Torr similar to FI of N_2, suggesting that a reduction in current could happen at higher pressures.

C. Characteristics Stability

Fig. 8 shows the shift in device characteristics during FI of N_2 at 10 Torr. The device was biased at 160 V generating initial collector current of 50 pA. The collector current gradually decreased to 15 pA after 10 000 s of FI at $V_{\mathrm{IG}} = 160$ V. The gate current remained relatively constant at ~1.5 μA throughout the experiment. The gradual current drop could be due to adsorption of molecules at the surface of the ionizer tip. These adsorbed molecules could form a surface layer that screens the electric field of the ionizer tip and reduces the effective field factor of the device. If the degradation of the device is due to particle adsorption at the surface, the device characteristics should be recoverable by removing the adsorbed layer. This can be performed by operating the device as a field emitter in high vacuum ($<10^{-7}$ Torr). Fig. 9(a) shows the change in FE characteristics of the device after continuous operation as field ionizer in N_2. The device was biased at a constant emitter current by controlling the gate-to-tip voltage. To maintain the emission current at a constant value, gate-to-tip voltage was gradually reduced. This is consistent with desorption of particles from the surface of the emitter tip observed by others [34], [35]. Fig. 9(b) confirms

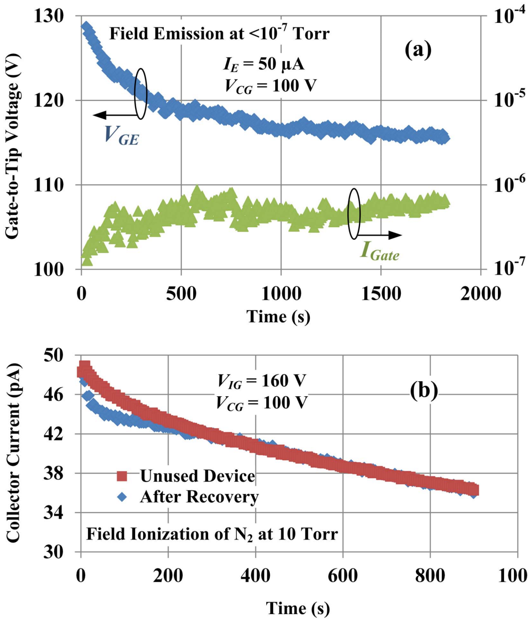

Fig. 9. (a) Characteristics shift of the device operating as a field emitter after continuous FI of N_2 at 10 Torr for 10^4 s. (b) Collector current as a function of time during FI of N_2 at 10 Torr using a fresh and recovered device; the device performance was recovered by operating the device as a field emitter at 10^{-7} Torr for 1800 s.

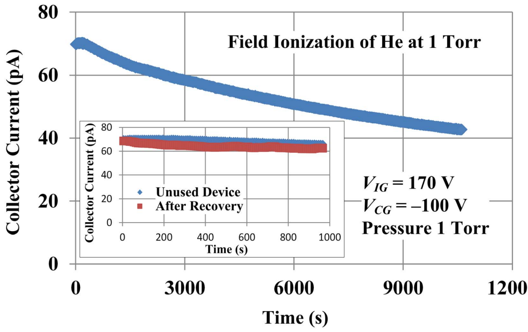

Fig. 10. FI of He: collector current versus time at 1 Torr and constant tip bias of 170 V. Inset confirms recovery of the device characteristics after FE at low pressures.

the recovery of the device characteristics after operation as a field emitter for 1800 s with constant emitter current of 50 μA at 10^{-7} Torr. Similar ion currents were generated by the fresh device and the device recovered by FE treatment after prolong FI of N_2. Furthermore, the degradation of device characteristics after recovery closely followed the same trend as the fresh device.

Stability of the device characteristics during FI of He at 1 Torr was also investigated (Fig. 10). A fresh device was biased at a constant V_{IG} of 170 V to produce initial collector current of ~70 pA. After 10^4 s of operation, the collector current reduced to 42 pA. Degradation of this device was lower compared with the device employed for FI of N_2. While a ~40% reduction in ion current was measured for the device operated in He, the collector current of the device operated in N_2 decreased by ~70%. The slower degradation of this device could be due to the lower chamber pressure during the experiment and lower chemical reactivity of He compared with N_2. As shown in the inset of Fig. 10, the device characteristics were recovered by operating the device as a field emitter at a high vacuum (<10^{-7} Torr). The device was biased for 1800 s at a constant emission current of 50 μA similar to the treatment applied to the device used for FI of N_2 [Fig. 9(a)].

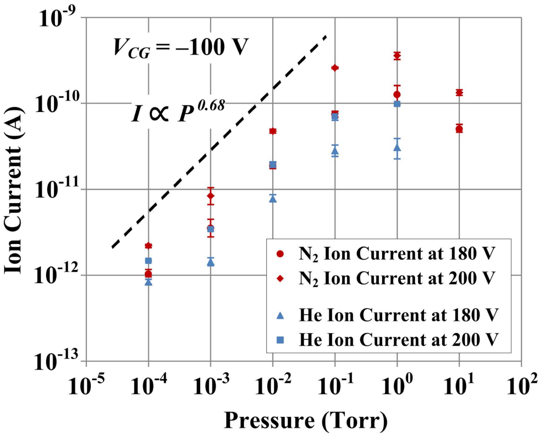

Fig. 11. Ion current versus pressure generated by FI of N_2 and He at ionizer tip-to-gate (V_{IG}) biases of 180 and 200 V.

V. DISCUSSION

FI current can be calculated from the product of ionization probability and the arrival rate of molecules to the high field region near the tip. Using Wentzel-Kramer-Brillouin approximation, the ionization probability is given by [5]

$$D \cong \exp\left[-6.8 \times 10^7 (I^{3/2} - \phi^{3/2})\alpha_I / F\right]. \qquad (6)$$

The term α_I accounts for the barrier lowering effect by image potential. If a constant ionization probability is assumed for a tip biased at a fixed potential, the ionization current must increase linearly with pressure as the flux of molecules to the tip is also a linear function of the pressure. Furthermore, except at very high fields in which every arriving molecule is ionized, the ionization probability and the ion current must be exponentially related to the ionization potential I.

Fig. 11 shows the collector currents as a function of chamber pressure generated by FI of He and N_2 at V_{IG} of 180 and 200 V. Each point on the graph is the average value calculated from five consecutive V_{IG} sweeps of 0–200–0 V recorded with a voltage step of 2 V. In all experiments, the collector-to-gate voltage was -100 V. Interestingly, the collector current did not exhibit a linear pressure dependence in the wide measurement range used in these experiments. Indeed, a weaker than linear dependence was observed in the pressure range 10^{-4}–10^{-1} Torr followed by saturation of the FI current at 1 Torr for both He and N_2 gases. Furthermore, a smaller collector current was achieved in N_2 at 10 Torr pressure compared with the measurement carried out at 1 Torr.

At 1 mTorr, the number of N_2 molecules arriving at the tip apex (area = 1 nm^2) is calculated to be >600 s^{-1} while the number of ions generated by each tip is <200 s^{-1} ($\sim I|_{V=200}$ at 1 mTorr divided by $320\,000q$). From this calculation, the ionization efficiency, η_I, defined as the ratio of generated ions to arriving molecules is <0.3 at 1 mTorr. Moreover, η_I decreases with pressure to <0.002 at 1 Torr and less than

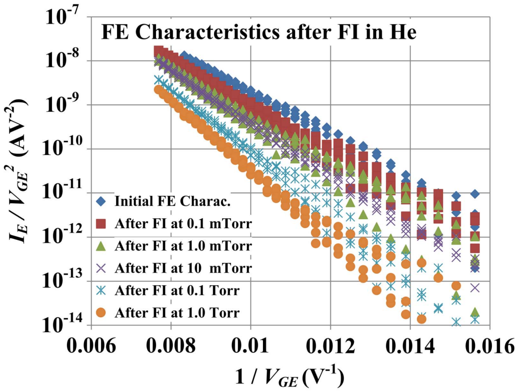

Fig. 12. FN plot of FE current measured before and after FI of He at different chamber pressures.

TABLE I

FE CHARACTERISTICS OF THE DEVICE BEFORE AND AFTER FI OF N_2 AND HE AT DIFFERENT PRESSURES

	FI in N_2		FI in He	
Condition	$a_{FN}/a_{0\,N2}$	$b_{FN}/b_{0\,N2}$	$a_{FN}/a_{0\,He}$	$b_{FN}/b_{0\,He}$
Initial FE Characteristics	1.0	1.00	1.0	1.00
After FI at 0.1 mTorr	1.1	1.32	0.6	1.02
After FI at 1 mTorr	1.9	1.41	1.2	1.13
After FI at 10 mTorr	5.7	1.54	1.3	1.16
After FI at 0.1 Torr	6.7	1.64	2.8	1.35
After FI at 1 Torr	2.8	1.65	5.0	1.48
After FI at 10 Torr	4.8	1.79	-	-

$a_{0\,N2} = 0.90\times10^{-4}$ AV^{-2} $b_{0\,N2} = 1008$ V
$a_{0\,He} = 2.08\times10^{-4}$ AV^{2} $b_{0\,He} = 1159$ V

10^{-4} at 10 Torr. A similar trend was also observed for FI of He. This implies that the ionization process is a barrier limited process rather than a supply limited phenomenon. Moreover, the probability of ionization degrades at higher pressures.

Another important observation was that the collector currents achieved during FI of He and N_2 at similar tip biases were close in magnitude. Despite the large difference in ionization potential of N_2 (14.6 eV) and He (25.4 eV), the ion currents are within a factor of 3 at all pressures and applied biases. This is not consistent with widely accepted FI theory, which predicts an exponential relation between ion current and the ionization potential particularly at low tip voltages where the FI current is limited by the tunneling process.

A possible explanation for the observed behavior is the formation of an adsorbed layer with a varying surface coverage depending on pressure, tip bias, and gas properties. As suggested earlier, formation of a surface layer can explain the degradation of the field ionizer during continuous operation. Furthermore, different degradation rates were observed for experiments performed in He and N_2.

Adsorption of particles on the surface of a field emitter is known to degrade the device characteristics [34], [35]. Here, we observed a similar degradation in FE performance of the fabricated devices after they were operated as field ionizers. Measurement of the FE characteristics of devices was carried out at pressures $<10^{-7}$ Torr to minimize the tip damage by back-streaming ions. Since the device characteristics recover quickly as shown in Fig. 9(a), the FE measurements were performed with a single back and forth 0–140 V sweep, a voltage step of 2 V, and a short hold time of 100 ms at each point. Fig. 12 shows the FN plots of the FE current measured immediately after FI experiments carried out at different pressures in He. The extracted FE characteristics of this device as well as a device operated in N_2 are presented in Table I. The a_{FN} and b_{FN} values are related to the field factor and work function of the tip material as expressed by (4) and (5). The b_{FN} value increased for both devices implying reduction of the field factor and/or increase of the material work function. As expected, both devices degraded more after FI at higher pressures.

A more pronounced impact was also observed on FE characteristics of the device operated in N_2. Furthermore, the degradation of this device can occur at lower pressures compared with the device used for FI of He. For instance, b_{FN} increased by $\sim$30% at pressures as low as 0.1 mTorr in N_2, while the corresponding change of b_{FN} was less than 3% in He. The value of a_{FN} was also increased for both devices after FI of He or N_2. This can be attributed to higher degradation of sharper tips than those having larger radius. In a large array, the extracted a_{FN} can be approximated by the sum of a_{FN} values of the tips weighted by their current contribution, i.e., the ratio of the tip current to the total emitted current. However, the emission current is mainly produced by a small fraction of sharper tips because of exponential dependence of the current to the field factor. Therefore, the extracted a_{FN}, is approximately the sum of a_{FN} values for a small group of sharp tips in the array. On the other hand, a_{FN} is a much weaker function of the tip radius compared with the emission current. When sharper tips are degraded, the tips with larger radius participate more effectively in the FE. Consequently, the extracted a_{FN} is increased as the current comes from larger number of the tips despite the reduction in total current. Although the degradation mechanism observed here is different, the shift in a_{FN} value is similar to the irreversible degradation of large arrays due to burn-out of the sharper tips at high emission currents [36].

The observed degradation in FE performance of the fabricated devices is a reversible phenomenon that is consistent with adsorption and desorption of molecules on the emitting surfaces of the device. This hypothesis is further supported with continuous FI measurement and recovery of the device characteristics by FE at low pressures. Furthermore, higher and faster degradation of the device was observed in N_2 as expected from adsorption of more nitrogen molecules on the tip surface compared with He [37], [38]. However, further experiments are needed to quantitatively study the degradation of device characteristics with respect to applied electric field, pressure, and duration of FI experiment.

VI. CONCLUSION

Pt-coated self-aligned gated tip arrays were designed and fabricated for FI of gasses at torr-level pressures and tip-to-gate voltages as low as 150 V. Photolithography and oxidation sharpening were employed to produce a self-aligned device configuration and highly uniform gate and tip dimensions. The fabricated devices are composed of 320 000 tips in 32 mm^2 and demonstrate average field factor $>10^6$ cm^{-1}. Such high field factors were generated by tips with radii <5 nm surrounded by individual gates with 1.5-μm radius of aperture. Our devices can produce ion currents as high as 0.35 nA and demonstrated stable characteristics for 10^4 s at 10 Torr. However, the device characteristics gradually degrades during the FI experiment but can be reestablished by operating the device as a field emitter at pressures below 10^{-7} Torr. This reversible degradation of the device characteristics is attributed to adsorption and desorption of gases on the tip surface. Irrespective of the underling mechanism, recovery of the device characteristics is very attractive for practical applications. Moreover, the low-voltage and high-pressure operation of these devices significantly reduces the power required for pumping and FI, rendering the disclosed devices excellent ion sources for portable analytical instruments.

REFERENCES

[1] H. D. Beckey, "Determination of the structures of organic molecules and quantitative analyses with the field ionization mass spectrometer," *Angew. Chem. Int. Ed.*, vol. 8, no. 9, pp. 623–688, Sep. 1969.

[2] M. Anbar and W. H. Aberth, "Field ionization mass spectrometry: A new tool for the analytical chemist," *Anal. Chem.*, vol. 46, no. 1, pp. 59A–64A, Jan. 1974.

[3] M. G. Inghram and R. Gomer, "Mass spectrometric analysis of ions from the field microscope," *J. Chem. Phys.*, vol. 22, no. 7, pp. 1279–1280, Jul. 1954.

[4] H. D. Beckey, *Principles of Field Ionization and Field Desorption Mass Spectrometry*. New York, NY, USA: Pergamon, 1977.

[5] R. Gomer, *Field Emission and Field Ionization*. New York, NY, USA: AIP, 1993.

[6] E. M. Chait, "Ionization sources in mass spectrometry," *Anal. Chem.*, vol. 44, no. 3, pp. 77A–91A, Mar. 1972.

[7] D. J. Riley *et al.*, "Helium detection via field ionization from carbon nanotubes," *Nano Lett.*, vol. 3, no. 10, pp. 1455–1458, 2003.

[8] K. Qian and G. J. Dechert, "Recent advances in petroleum characterization by GC field ionization time-of-flight high-resolution mass spectrometry," *Anal. Chem.*, vol. 74, no. 16, pp. 3977–3983, Aug. 2002.

[9] B. Reichenbach, I. Solano, and P. R. Schwoebel, "A field evaporation deuterium ion source for neutron generators," *J. Appl. Phys.*, vol. 103, no. 9, pp. 094912-1–094912-4, May 2008.

[10] A. Persaud *et al.*, "Development of a compact neutron source based on field ionization processes," *J. Vac. Sci. Technol. B*, vol. 29, no. 2, pp. 02B107-1–02B107-4, Mar. 2011.

[11] E. de Hoffmann and V. Stroobant, *Mass Spectrometry: Principles and Applications*, 3rd ed., Hoboken, NJ, USA: Wiley, 2007.

[12] L. Gao, Q. Y. Song, G. E. Patterson, R. G. Cooks, and Z. Ouyang, "Handheld rectilinear ion trap mass spectrometer," *Anal. Chem.*, vol. 78, no. 17, pp. 5994–6002, Sep. 2006.

[13] C. A. Bower *et al.*, "On-chip electron-impaction source using carbon nanotube field emitters," *Appl. Phys. Lett.*, vol. 90, no. 12, pp. 124102-1–124102-3, Mar. 2007.

[14] L. F. Velasquez-Garcia, B. L. P. Gassend, and A. I. Akinwande, "CNT-based MEMS/NEMS gas ionizers for portable mass spectrometry applications," *J. Microelectromech. Syst.*, vol. 19, no. 3, pp. 484–493, Jun. 2010.

[15] C. A. Spindt, "Microfabricated field-emission and field-ionization sources," *Surf. Sci.*, vol. 266, no. 1, pp. 145–154, Apr. 1992.

[16] J. H. Gross, *Mass Spectrometry: A Textbook*, Heidelberg, Germany: Springer-Verlag, 2006.

[17] L.-Y. Chen, L. F. Velásquez-García, X. Wang, K. Teo, and A. I. Akinwande, "A microionizer for portable mass spectrometers using double-gated isolated vertically aligned carbon nanofiber arrays," *IEEE Trans. Electron Device*, vol. 58, no. 7, pp. 2149–2158, Jul. 2011.

[18] R. Gomer, "Field emission, field ionization, and field desorption," *Surf. Sci.*, vols. 299–300, pp. 129-152, Jan. 1994.

[19] E. W. Müller, *Advances in Electronics and Electron Physics*. New York, NY, USA: Academic, 1960.

[20] K. Edinger, V. Yun, J. Melngailis, J. Orloff, and G. Magera, "Development of a high brightness gas field ion source," *J. Vac. Sci. Technol. B*, vol. 15, no. 6, pp. 2365–2368, Dec. 1997.

[21] K. Jousten, K. Bohringer, R. Borret, and S. Kalbitzer, "Growth and current characteristics of stable protrusions on tungsten field ion emitters," *Ultramicroscopy*, vol. 26, no. 3, pp. 301–312, 1988.

[22] J. A. Kubby and B. M. Siegel, "High resolution structuring of emitter tips for the gaseous field ionization source," *J. Vac. Sci. Technol. B*, vol. 4, no. 1, pp. 120–125, Feb. 1986.

[23] W. Aberth and C. A. Spindt, "Characteristics of a volcano field ion quadrupole mass spectrometer," *Int. J. Mass Spectrometry Ion Phys.*, vol. 25, no. 2, pp. 183–198, Oct. 1977.

[24] L.-Y. Chen, L. F. Velásquez-García, X. Wang, K. Teo, and A. I. Akinwande, "A micro ionizer for portable mass spectrometers using double-gated isolated vertically aligned carbon nanofiber arrays," in *Proc. IEEE IEDM*, Dec. 2007, pp. 843–846.

[25] I. Solano *et al.*, "Field desorption ion source development for neutron generators," *Nucl. Instrum. Methods Phys. Res. Sec. A, Accel., Spectrometers, Detectors Assoc. Equip.*, vol. 587, no. 1, pp. 76–81, Mar. 2008.

[26] B. Bargsten Johnson, P. R. Schwoebel, C. E. Holland, P. J. Resnick, K. L. Hertz, and D. L. Chichester, "Field ion source development for neutron generators," *Nucl. Instrum. Methods Phys. Res. Sec. A, Accel., Spectrometers, Detectors Assoc. Equip.*, vol. 663, no. 1, pp. 64–67, Jan. 2012.

[27] P. J. Resnick, C. E. Holland, P. R. Schwoebel, K. L. Hertz, and D. L. Chichester, "An integrated field emission array for ion desorption," *Microelectron. Eng.*, vol. 87, nos. 5–8, pp. 1263–1265, Aug. 2010.

[28] K. B. K. Teo *et al.*, "Plasma enhanced chemical vapour deposition carbon nanotubes/nanofibres-how uniform do they grow?" *Nanotechnology*, vol. 14, no. 2, pp. 204–211, Feb. 2003.

[29] A. A. Fomani, S. A. Guerrera, L. F. Velasquez-Garcia, and A. I. Akinwande, "Toward AMP-level field emission with large-area arrays of Pt-coated self-aligned gated nano-scale tips," to be published.

[30] M. Ding, H. Kim, and A. I. Akinwande, "Highly uniform and low turn-on voltage Si field emitter arrays fabricated using chemical mechanical polishing," *IEEE Electron Device Lett.*, vol. 21, no. 2, pp. 66–69, Feb. 2000.

[31] R. H. Fowler and L. Nordheim, "Electron emission in intense electric fields," *Proc. R. Soc. London Ser. A, Contain. Papers Math. Phys. Character*, vol. 119, no. 781, pp. 173–181, Mar. 1928.

[32] C. A. Spindt, I. Brodie, L. Humphrey, and E. R. Westerberg, "Physical properties of thin-film field emission cathodes with molybdenum cones," *J. Appl. Phys.*, vol. 47, no. 12, pp. 5248–5263, Dec. 1976.

[33] J. A. Rees, *Electrical Breakdown in Gases*. New York, NY, USA: Wiley, 1973.

[34] M. S. Mousa, P. R. Schwoebel, I. Brodie, and C. A. Spindt, "Observations of work function changes in field-emitter arrays," *Appl. Surf. Sci.*, vol. 67, nos. 1–4, pp. 56–58, Apr. 1993.

[35] D. Temple, W. D. Palmer, L. N. Yadon, J. E. Mancusi, D. Vellenga, and G. E. McGuire, "Silicon field emitter cathodes: Fabrication, performance, and applications," *J. Vac. Sci. Technol. A*, vol. 16, no. 3, pp. 1980–1990, Jun. 1998.

[36] L. F. Velasquez-Garcia, S. A. Guerrera, Y. Niu, and A. I. Akinwande, "Uniform high-current cathodes using massive arrays of Si field emitters individually controlled by vertical Si ungated FETs—Part 1: Device design and simulation," *IEEE Trans. Electron Dev.*, vol. 58, no. 6, pp. 1775–1782, Jun. 2011.

[37] W. V. Loebenstein and V. R. Deitz, "Surface-area determination by adsorption of nitrogen from nitrogen-helium mixtures," *J. Res. Nat. Inst. Stand. Technol.*, vol. 46, pp. 51–55, Jan. 1951.

[38] R. Hellemans, A. Van Itterbeek, and W. Van Dael, "The adsorption of helium, argon and nitrogen on graphite," *Physica*, vol. 34, no. 3, pp. 429–438, 1967.

Arash A. Fomani (S'03–M'12) is a Post-Doctoral Associate with the Microsystems Technology Laboratories, Massachusetts Institute of Technology, Cambridge, MA, USA. His current research interests include the design, fabrication, and reliability of MEMS, vacuum nanoelectronics, and semiconductor devices for portable analytical instruments, biomedical equipment, and sensing systems.

Luis Fernando Velásquez-García (M'09–SM'10) is a Principal Scientist with the Microsystems Technology Laboratories, Massachusetts Institute of Technology, Cambridge, MA, USA, and an expert in micro and nanofabrication. His current research interests include micro and nanoenabled multiplexed scaled-down systems that exploit high-electric field phenomena for space, energy, healthcare, manufacturing, and analytical applications.

Akintunde Ibitayo (Tayo) Akinwande (S'81–M'86–SM'04–F'08) is a Professor with the Department of Electrical Engineering and Computer Science, Massachusetts Institute of Technology, Cambridge, MA, USA. His current research interests include intelligent displays, large-area electronics, and microscale devices based on charged particle beams, such as chip-scale mass spectrometers, field ionizers, and field emission cathodes.